

Optical characteristics of excitons in $\text{In}_{1-x}\text{Ga}_x\text{As}_y\text{P}_{1-y}/\text{InP}$ quantum wells

M. Sugawara, T. Fujii, S. Yamazaki, and K. Nakajima

Fujitsu Laboratories Ltd., 10-1, Morinosato-Wakamiya, Atsugi 243-01, Japan

(Received 2 January 1991)

This paper presents a systematic study on the optical characteristics of ground-state electron-heavy-hole excitons in $\text{In}_{1-x}\text{Ga}_x\text{As}_y\text{P}_{1-y}/\text{InP}$ quantum wells, specifically focusing on the resonance energy, spatial energy inhomogeneity, and optical-absorption strength. The exciton resonance energy can be predicted by conventional effective-mass equations. The low-temperature broadening of the photoluminescence spectrum was studied in relation to the composition of $\text{In}_{1-x}\text{Ga}_x\text{As}_y\text{P}_{1-y}$ and the excitation power density. We show the composition of $\text{In}_{1-x}\text{Ga}_x\text{As}_y\text{P}_{1-y}$ fluctuates not only statistically within the exciton volume but also macroscopically, which is the primary cause for the inhomogeneous broadening of the exciton resonance in $\text{In}_{1-x}\text{Ga}_x\text{As}_y\text{P}_{1-y}/\text{InP}$ quantum wells. The exciton migration over macroscopically fluctuating $\text{In}_{1-x}\text{Ga}_x\text{As}_y\text{P}_{1-y}$ and its preferential recombination in the lower-energy regions is discussed based on our calculation of the exciton lifetime. The integrated intensity of the optical-absorption spectrum of exciton resonance was found to increase as the well band gap increased. Our theoretical formula indicates that this band-gap dependence is quantitatively correlated with the two-dimensional-exciton radius. We show that both the exciton radius and the magnitudes of composition fluctuations primarily determine the exciton optical-absorption strength in $\text{In}_{1-x}\text{Ga}_x\text{As}_y\text{P}_{1-y}/\text{InP}$ quantum wells.

I. INTRODUCTION

Semiconductor quantum wells are fabricated by layering different thin semiconductor films and controlling the potential profile in the conduction and valence bands.¹ The motion of electrons and holes confined in the quantum wells is effectively restricted to two dimensions,² giving rise to various physical phenomena not observable in bulk materials. The most striking optical characteristic is that exciton optical-absorption resonances can be observed even at room temperature. This was first found in GaAs/ $\text{Al}_{1-x}\text{Ga}_x\text{As}$ quantum wells.³ The Stark shift⁴ and the large optical nonlinearity⁵ of the exciton resonances enable the modulation of the dielectric constants in quantum wells to a much greater extent than in bulk materials, making it possible to develop additional optical devices such as high-speed optical modulators,⁶ optical switches,⁷ optical bistable devices [self-generated electro-optic effect devices (SEED's)],⁸ and bistable lasers.⁹

The combination of InP barriers with $\text{In}_{1-x}\text{Ga}_x\text{As}_y\text{P}_{1-y}$ wells lattice matched to InP is the most attractive candidate for making devices that work in optical communication systems since the ground-state exciton energy can be tuned to around 1.3 and 1.55 μm (Ref. 10). High-quality quantum-well structures have been frequently reported in the literature because of the recent progress in gas-phase growth techniques such as metalorganic vapor-phase epitaxy (MOVPE),¹¹⁻¹⁹ gas-source molecular-beam epitaxy,^{20,21} and chemical-beam epitaxy.²² Exciton resonances^{16,17,23,24} and their Stark shift^{25,26} were observed in the room-temperature optical-absorption spectra. To develop new optical devices using $\text{In}_{1-x}\text{Ga}_x\text{As}_y\text{P}_{1-y}/\text{InP}$ quantum wells, the exciton characteristics specific to this quantum-well system must

be known, as well as the characteristics dependent on the composition of $\text{In}_{1-x}\text{Ga}_x\text{As}_y\text{P}_{1-y}$ wells. Sufficient knowledge of these topics has not been acquired.

This work presents a systematic study of the ground-state electron-heavy-hole exciton resonance in $\text{In}_{1-x}\text{Ga}_x\text{As}_y\text{P}_{1-y}/\text{InP}$ quantum wells, specifically focusing on the resonance energy, spatial energy inhomogeneity, and optical-absorption strength. Exciton resonances in low-temperature photoluminescence spectra and optical-absorption spectra are analyzed. We present a theoretical formula for the exciton recombination lifetime, in addition to the exciton optical-absorption spectrum derived in our previous work.²⁷ We show that the composition of our $\text{In}_{1-x}\text{Ga}_x\text{As}_y\text{P}_{1-y}$ layers fluctuates not only statistically within the exciton volume but also macroscopically, which is the primary cause for inhomogeneous broadening of the resonance spectrum in our quantum wells. Migration of excitons through alloys with macroscopically fluctuating compositions and their preferential recombination in lower-energy regions is quantitatively discussed based on our calculation of exciton lifetime. The integrated intensity of the optical-absorption spectra of exciton resonances is correlated with the band gap of well materials and also with the two-dimensional exciton radius. We show that the exciton optical-absorption strength, dependent on $\text{In}_{1-x}\text{Ga}_x\text{As}_y\text{P}_{1-y}$ composition, is dominated by the two-dimensional exciton radius and the magnitude of composition fluctuations.

II. EXPERIMENT

The samples studied were undoped $\text{In}_{1-x}\text{Ga}_x\text{As}_y\text{P}_{1-y}$ layers, $\text{In}_{1-x}\text{Ga}_x\text{As}_y\text{P}_{1-y}/\text{InP}$ single quantum wells, and periodic multiple quantum wells (MQW's). We first grew

undoped 200-nm InP buffer layers on (100)-oriented InP substrates, followed by the samples by low-pressure MOVPE. The growth temperature was around 600 °C. The In, Ga, As, and P sources were trimethylindium, triethylgallium, arsine, and phosphine. Pd-diffused high-purity hydrogen was the carrier gas. The total carrier-gas flow rate was 6 liters per minute. The As composition was $y=1.0, 0.9,$ and 0.6 in the quantum wells. The double-crystal x-ray-diffraction measurements revealed the bulk $\text{In}_{1-x}\text{Ga}_x\text{As}_y\text{P}_{1-y}$ layers are closely lattice matched to InP, satisfying the relation of $x=0.47y$. We grew a series of single $\text{In}_{1-x}\text{Ga}_x\text{As}_y\text{P}_{1-y}$ quantum wells with different well widths, each separated by 50-nm InP layers. Also, a 200-nm bulk $\text{In}_{1-x}\text{Ga}_x\text{As}_y\text{P}_{1-y}$ layer was grown on an InP substrate. The well width L_W varied from 1 to 20 nm. The MQW's consist of alternating 10-nm $\text{In}_{1-x}\text{Ga}_x\text{As}_y\text{P}_{1-y}$ wells and 10-nm InP barriers for 20 periods.

In one period of a MQW, the well and barrier layer thicknesses were determined by analyzing small-angle x-ray-diffraction patterns.^{28,29} Using these measured thicknesses and the growth times, we determined the average growth rate of the $\text{In}_{1-x}\text{Ga}_x\text{As}_y\text{P}_{1-y}$ and InP layers. For single quantum wells, the thickness of the well layers was estimated from the growth time.

We measured the photoluminescence spectra of our samples at 4.2 K. A 647.1-nm Kr^+ laser was used to excite samples immersed in liquid He. The diameter of the focused laser beam was estimated to be about 250 μm from the reflected intensity profile on the wafer edge. The excitation power density was varied between 500 and 0.5 W/cm^2 . Photoluminescence was dispersed by a 50-cm monochromator and detected by a PbS detector using a conventional lock-in technique.

We measured the optical-absorption spectra of MQW's at 77 and 295 K. The light of a halogen lamp dispersed by a 32-cm monochromator was focused to a diameter of 250 μm on the MQW samples. The light transmitted through the sample was detected using a PbS detector and a lock-in amplifier. The optical absorbance of a quantum well, αL_{QW} , was determined by $\alpha L_{\text{QW}} = (1/N) \ln(I_2/I_1)$, where I_1 and I_2 are the intensities of the light transmitted from a sample and from an InP substrate and N is the number of the wells. Taking the period in a MQW structure as L_{QW} , α represents the average optical-absorption coefficient of a quantum well.

III. EXCITON ENERGY

In photoluminescence measurements, electrons and holes are excited by photon absorption high into the conduction and valence bands and relax to the band edges by the phonon scattering within a time of about 1 ps (Ref. 30). At the liquid-He temperature 4.2 K, the exciton binding energy is larger than the thermal energy kT in III-V semiconductors, and excitons are formed according to the thermodynamic equilibrium as the lowest excited states.^{31,32} Figure 1 shows the typical 4.2-K photoluminescence spectra of stacks of quantum wells and a 200-nm bulk layer of ternary $\text{In}_{0.53}\text{Ga}_{0.47}\text{As}$ ($y=1.0$) successively grown on an InP substrate. The width of

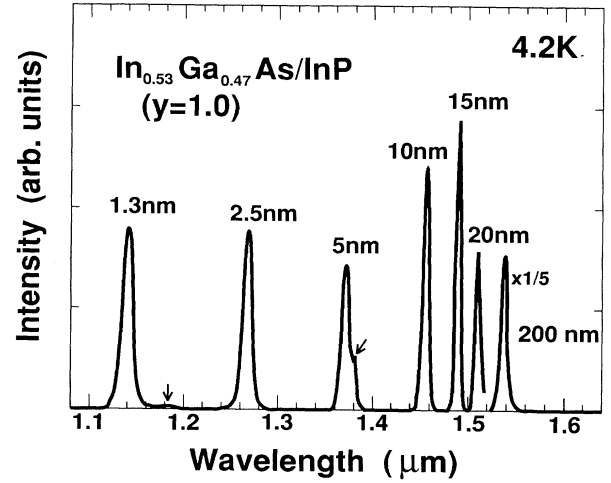


FIG. 1. Photoluminescence spectra of stacks of $\text{In}_{0.53}\text{Ga}_{0.47}\text{As}/\text{InP}$ single quantum wells and a 200-nm bulk layer at 4.2 K. The widths of $\text{In}_{0.53}\text{Ga}_{0.47}\text{As}$ layers are estimated to be 1.3, 2.5, 5, 10, 15, and 20 nm. The InP barrier layers are 50 nm thick. The sharp lines can be attributed to the ground-state electron-heavy-hole exciton recombinations.

$\text{In}_{0.53}\text{Ga}_{0.47}\text{As}$ is 1.3, 2.5, 5, 10, 15, 20, and 200 nm. We can attribute sharp lines to the ground-state exciton recombinations and the peak energy to the exciton energy in each quantum well and a bulk layer. The spectra of the 5- and 1.3-nm quantum wells have subpeaks at the lower-energy side of the main spectrum as designated by arrows. The splitting energy of the sub and main peaks is about 5 meV in the 5-nm quantum well and about 37 meV in the 1.3-nm quantum well. Such subpeaks that appear in low-temperature photoluminescence have been studied extensively in the literature^{33,34} and are attributed to the recombination of excitons in monolayer thicker area whose lateral size exceeds the extent of the exciton's two-dimensional wave functions.

Figure 2 plots the peak energy of 4.2-K photoluminescence main spectra as a function of the width of $\text{In}_{1-x}\text{Ga}_x\text{As}_y\text{P}_{1-y}$ in quantum wells. The arsenic composition is $y=1.0, 0.9,$ and 0.6 . The peak shifts from the band gap of bulk $\text{In}_{0.53}\text{Ga}_{0.47}\text{As}$ (0.808 eV) toward higher energy as the arsenic composition y decreases due to the increase in the band gap of the $\text{In}_{1-x}\text{Ga}_x\text{As}_y\text{P}_{1-y}$ wells and as the well width decreases due to the quantum confinement effect. The solid lines represent the exciton energy calculated by the effective-mass equation:³⁵

$$E_{\text{ex}} = E_g + \langle \psi_e(z_e) | H_e | \psi_e(z_e) \rangle + \langle \psi_h(z_h) | H_h | \psi_h(z_h) \rangle + \langle \Phi | H_r | \Phi \rangle, \quad (1)$$

$$H_e = -\frac{\hbar^2}{2m_e} \frac{\partial^2}{\partial z_e^2} + V_e(z_e), \quad (2)$$

$$H_h = -\frac{\hbar^2}{2m_h} \frac{\partial^2}{\partial z_h^2} + V_h(z_h), \quad (3)$$

$$H_r = -\frac{\hbar^2}{2\mu}\Delta_r - \frac{e^2}{4\pi\epsilon}[r^2 + (z_e - z_h)^2]^{-1/2}, \quad (4)$$

$$\Phi = \frac{1}{\sqrt{D}} e^{i\mathbf{K}\cdot\mathbf{R}} \phi_{\text{ex}}(\mathbf{r}) \psi_e(z_e) \psi_h(z_h), \quad (5)$$

where E_g is the band gap of $\text{In}_{1-x}\text{Ga}_x\text{As}_y\text{P}_{1-y}$, \hbar is Planck's constant divided by 2π , z_e and z_h are the perpendicular coordinates to the quantum-well layers of an electron and a hole, respectively, r is the in-plane distance between an electron and a hole, m_e is the effective mass of an electron, m_h is the effective mass of a hole in the direction perpendicular to the quantum well, μ is the in-plane exciton reduced effective mass, Φ is the envelope function of excitons, $V_e(z_e)$ and $V_h(z_h)$ are the quantum-well potentials in the conduction and valence bands, respectively, e is the charge of an electron, ϵ is the static dielectric constant, $\psi_e(z_e)$ is the electron envelope wave function describing confined states, $\psi_h(z_h)$ is the hole's wave function, \mathbf{R} is the in-plane center of mass of an electron and a hole, \mathbf{K} is the wave vector of its motion, and D is the area of the quantum well. We use³⁵

$$\phi_{\text{ex}}(\mathbf{r}) = \left(\frac{2}{\pi}\right)^{1/2} \frac{1}{\lambda_{\text{ex}}} e^{-r/\lambda_{\text{ex}}} \quad (6)$$

to describe the in-plane motion of excitons, where λ_{ex} represents the two-dimensional exciton radius. On the right-hand side of Eq. (1), the second and third terms represent the quantum confinement energy of an electron and a hole, respectively. The fourth term represents the exciton binding energy, which can be calculated variationally by³⁵

$$E_B(\lambda_{\text{ex}}) = \frac{\hbar^2}{2\mu\lambda_{\text{ex}}^2} - \frac{e^2}{4\pi\epsilon} \left\langle \Phi \left| \frac{1}{\rho} \right| \Phi \right\rangle, \quad (7)$$

where $\rho = [r^2 + (z_e - z_h)^2]^{1/2}$. The discontinuity in the conduction band between InP and $\text{In}_{1-x}\text{Ga}_x\text{As}_y\text{P}_{1-y}$ was assumed to be 40% of the band-gap difference, and 60% in the valence band.³⁶ In our calculations, we used the material parameters of bulk $\text{In}_{1-x}\text{Ga}_x\text{As}_y\text{P}_{1-y}$. The effective masses of electrons and holes are obtained by a linear interpolation of the values listed by Pearsall:³⁷ $m_e = 0.041m_0$ and $m_h = 0.5m_0$ for $y = 1.0$, $m_e = 0.044m_0$ and $m_h = 0.5m_0$ for $y = 0.9$, $m_e = 0.053m_0$ and $m_h = 0.5m_0$ for $y = 0.6$, and $m_e = 0.08m_0$ and $m_h = 0.56m_0$ for InP. We estimated the dielectric constants by a linear interpolation between $\epsilon = 13.9\epsilon_0$ for $\text{In}_{0.53}\text{Ga}_{0.47}\text{As}$ ($y = 1.0$) and $\epsilon = 12.4\epsilon_0$ for InP ($y = 0$) (Ref. 38). (These material parameters are used also in Sec. IV to calculate the magnitudes of statistical composition fluctuations.)

The equations satisfactorily explain the dependence of the exciton energy on the composition and the well width. In particular, when wells are thicker than 10 nm, Eqs. (1)–(7) can precisely predict the energy shift. Both experimental and theoretical results show that the exciton energy can be continuously tuned between $\text{In}_{0.53}\text{Ga}_{0.47}\text{As}$ and InP by controlling the composition of $\text{In}_{1-x}\text{Ga}_x\text{As}_y\text{P}_{1-y}$ and/or the well width. Its wavelength is what we need for the devices that work in optical communication systems. The important characteristics of quantum wells such as the density of state per unit volume,² the oscillator strength of exciton transitions,³⁹ and the Stokes shift of exciton resonance³⁵ strongly depend on the well width. Thus, the width should be preferentially optimized for each device to attain excellent performance. Using quaternary $\text{In}_{1-x}\text{Ga}_x\text{As}_y\text{P}_{1-y}$ as a well material, we can control the exciton energy by changing the composition of the quaternary well along the lattice-matching condition of $x = 0.47y$ with an optimal well width.

In thinner quantum wells, the measured points fall below the theoretical lines, as often found by others.¹⁵ Morais *et al.*³⁴ studied multiple peak spectra that appeared in low-temperature photoluminescence of very thin single quantum wells. They attributed these spectra to the exciton recombinations in two- to six-monolayer islands and showed that the energy shift agreed well with the theory. The discrepancy in our quantum wells between the theoretical and experimental results may have

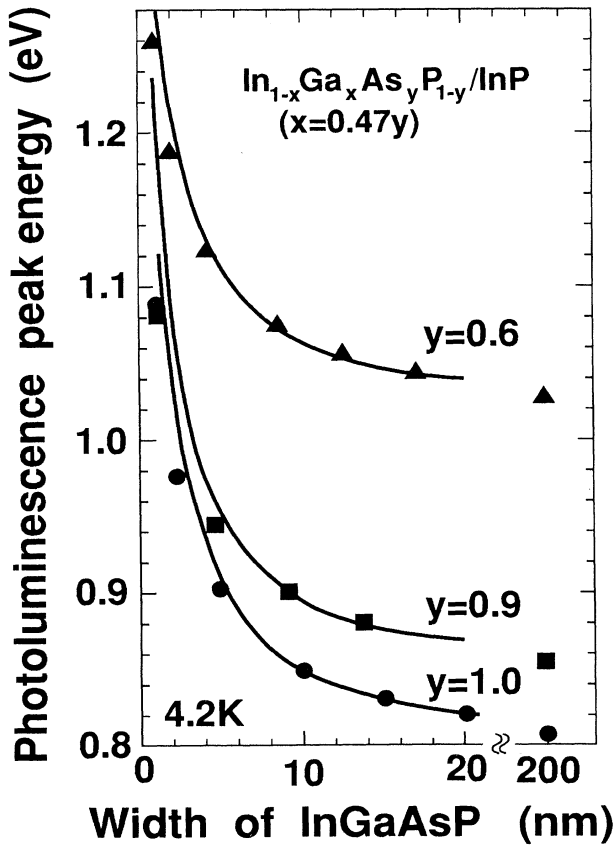


FIG. 2. Photoluminescence spectrum peak energy as a function of the width of $\text{In}_{1-x}\text{Ga}_x\text{As}_y\text{P}_{1-y}$ at 4.2 K. The arsenic composition of $\text{In}_{1-x}\text{Ga}_x\text{As}_y\text{P}_{1-y}$ is $y = 0.6, 0.9$, and 1.0 with $x = 0.47y$. The solid lines are the calculated results based on Eqs. (1)–(7).

been caused by the layer thickness being underestimated due to the nonlinear growth rate.

IV. INHOMOGENEOUS BROADENING

The broadening of low-temperature photoluminescence spectra represents the spatial inhomogeneity of the exciton energy. Figure 3 shows the photoluminescence spectrum width [full width at half maximum (FWHM)] as a function of the width of $\text{In}_{1-x}\text{Ga}_x\text{As}_y\text{P}_{1-y}$ single quantum wells and bulk layers. The spectra broadened as the well width and the arsenic composition y decreased. The composition dependence of the spectrum width is probably caused by the difference in the broadening among bulk $\text{In}_{1-x}\text{Ga}_x\text{As}_y\text{P}_{1-y}$ layers: 7.0 meV for $y=0.6$, 4.3 meV for $y=0.9$, and 3.0 meV for $y=1.0$.

Spectrum broadening in bulk layers can be attributed primarily to composition fluctuations. Since the exciton radius is on the order of 10 nm, the number of atoms included in the exciton volume is as small as 10^5 to 10^6 cm^{-3} ; excitons statistically “feel” composition fluctuations, resulting in inhomogeneous broadening of the exciton-resonance spectrum. According to Schubert *et al.*,⁴⁰ the statistical composition fluctuation in $\text{In}_{1-x}\text{Ga}_x\text{As}_y\text{P}_{1-y}$ causes a Gaussian-type broadening with the FWHM of

$$\Gamma_{\text{sta}} = [f(x)^2 + f(y)^2]^{1/2}, \quad (8)$$

where

$$f(x) = 2.35 \left[\frac{\partial E_g}{\partial x} \right] \left[\frac{x(1-x)}{KV_{3D}} \right]^{1/2}, \quad (9)$$

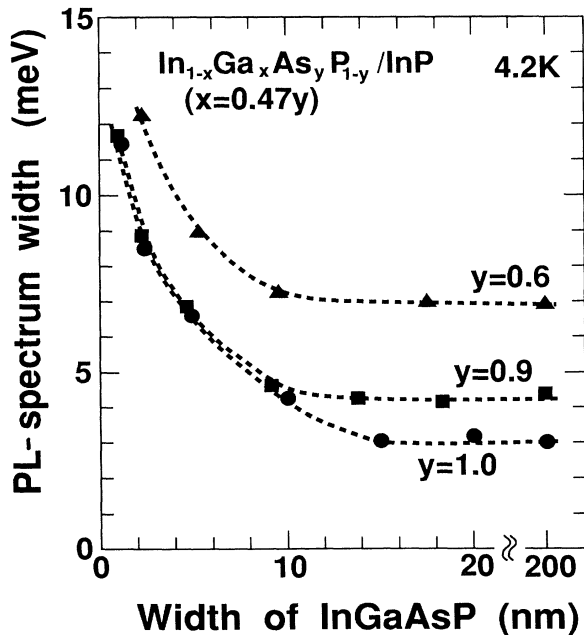


FIG. 3. Photoluminescence spectrum width (FWHM) at 4.2 K as a function of the width of $\text{In}_{1-x}\text{Ga}_x\text{As}_y\text{P}_{1-y}$. The arsenic composition is $y=1.0$, 0.9, and 0.6 with $x=0.47y$. The dashed lines are guides for the eye.

V_{3D} is the three-dimensional exciton volume, K is the density of group-III or group-V atoms, and $\partial E_g/\partial x$ is the change in the band-gap energy with the composition x .

In Fig. 4, we plotted both the calculated Γ_{sta} (solid line) and the measured photoluminescence spectrum width (open circles) at 4.2 K as a function of the arsenic composition y . In addition to the three bulk layers whose spectrum widths are shown in Fig. 3, we also plotted the results of other 0.5- μm bulk layers. Since the exciton envelope wave function of the relative motion in bulk materials is spherical, we assumed $V_{3D} = (4\pi/3)a^3$, where the three-dimensional exciton radius is given as $a = 0.053(m_0/\mu)(\epsilon/\epsilon_0)$ nm based on the effective-mass approximation.⁴¹ The calculated line has a maximum of about 4 meV around $y=0.3$ and is zero for binary InP. The measured widths are broader than the calculated ones, with the exception of the sample indicated as No. 1 in Fig. 4. Therefore, the results of photoluminescence measurements suggest that composition fluctuates not only statistically but also macroscopically over the 250- μm excited area.

We use the following model for macroscopic composition fluctuations. Bulk materials are divided into pieces whose volume is large enough to neglect the statistical fluctuations (a 100-nm cube, for example). Suppose that the average composition of $\text{In}_{1-x}\text{Ga}_x\text{As}_y\text{P}_{1-y}$ in each piece fluctuates according to a Gaussian distribution with a FWHM of Δx and Δy . The spectrum broadening due to the fluctuation can be written as

$$\Gamma_{\text{mac}} = \left[\left[\frac{\partial E_g}{\partial x} \right]^2 \Delta x^2 + \left[\frac{\partial E_g}{\partial y} \right]^2 \Delta y^2 \right]^{1/2}. \quad (10)$$

Assuming that the statistical broadening within the exciton volume in each piece does not vary, the exciton spectrum width (FWHM) in bulk layers can be written as

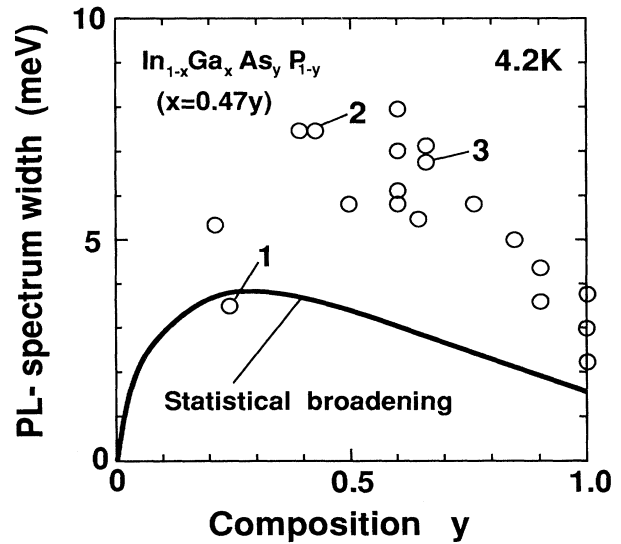


FIG. 4. The solid line represents the spectrum width (FWHM) of $\text{In}_{1-x}\text{Ga}_x\text{As}_y\text{P}_{1-y}$ bulk layers due to the statistical composition fluctuations as a function of the arsenic composition of y ($x=0.47y$). The open circles represent the measured 4.2-K photoluminescence spectrum widths.

$$\Gamma_{\text{com}} = (\Gamma_{\text{sta}}^2 + \Gamma_{\text{mac}}^2)^{1/2}. \quad (11)$$

Substituting the measured spectrum width for Γ_{com} and the calculated values for Γ_{sta} in Eq. (11), Γ_{mac} can be calculated. In the $\text{In}_{1-x}\text{Ga}_x\text{As}_y\text{P}_{1-y}$ bulk layers of Fig. 3, for example, the calculations yield 2.5 meV for $y=1.0$, 3.8 meV for $y=0.9$, and 6.3 meV for $y=0.6$. These fluctuations in energy correspond to several tens of angstroms in wavelength, around 1% in the group-III and/or group-V species from Eq. (10).

Macroscopic composition fluctuations could be detected by studying the excitation power dependence of the photoluminescence spectrum broadening. Figure 5 shows the 4.2-K photoluminescence spectrum width (FWHM) as a function of the excitation power for samples 1, 2, and 3 as designated in Fig. 4. The excitation power for the measurements used in Figs. 1–4 was above 200 W/cm^2 . The spectrum width of sample 1, which was almost identical to the calculated statistical broadening in Fig. 4, was almost independent of the excitation power. However, in samples 2 and 3, the spectrum gradually narrowed when the excitation power dropped below about 200 W/cm^2 ; below 10 W/cm^2 , the spectrum saturated. Figure 6 shows the photoluminescence spectra of (a) sample 1 at 490 W/cm^2 (solid line) and at 1.1 W/cm^2 (dashed line) and (b) sample 2 at 400 W/cm^2 (solid line) and at 1.0 W/cm^2 (dashed line). In both parts of this figure, the peak intensities are normalized. At high excitation power, both samples show almost symmetrical spectra approximating Gaussian distributions, except for the long tails on both sides. At low power, the spectrum of sample 2 lacks the shorter wavelength, becoming asymmetric, while the profile of sample 1 is almost unchanged. This excitation power dependence of the low-temperature photoluminescence spectrum profile was first reported by

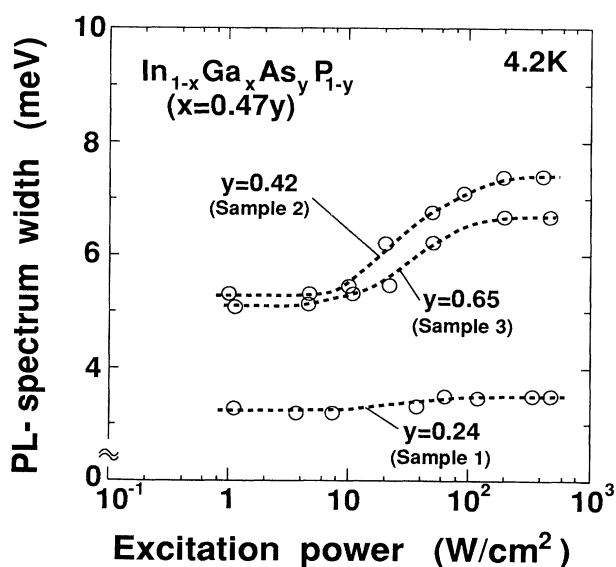


FIG. 5. Photoluminescence spectrum width (FWHM) at 4.2 K as a function of the excitation power density for samples 1, 2, and 3 indicated in Fig. 4.

Schubert and Tsang.⁴² They suggested that the recombination lifetime of excitons increased as the excitation power decreased, making the diffusion length of excitons longer, and that excitons recombine preferentially in the lower-energy regions. In their experiments, the saturation of the spectrum width at both higher and lower excitation intensities was not found. We will explain this phenomenon quantitatively as follows.

Based on the effective-mass approximation, the time-dependent perturbation theory, and Einstein's relation,⁴³ the radiative recombination rate of excitons per unit volume in bulk materials is given as

$$R(N_{\text{ex}}) = \frac{ne^2 E_{\text{ex}}}{\pi \epsilon_0 c^3 m_0^2 \hbar^2 V} \left| \sum_{\mathbf{k}} A(\mathbf{k}) P_{cv} f_c(\mathbf{k}) [1 - f_v(\mathbf{k})] \right|^2, \quad (12)$$

where c is the speed of light, n is the refractive index, V is the volume of bulk materials, and P_{cv} is the transition-matrix element between the conduction-band and valence-band Bloch states. An exciton state is formed by the linear combination of the product of single-particle Bloch states in the conduction and valence bands. $A(\mathbf{k})$ is its expansion coefficient, $f_c(\mathbf{k})$ and $f_v(\mathbf{k})$ are the Fermi-Dirac distribution functions in the conduction band and in the valence band, respectively, and \mathbf{k} is the wave vector. Note that the recombination rate is a function of the electron-hole pair density N_{ex} . Performing the summation in \mathbf{k} space, we could reduce Eq. (12) to

$$R(N_{\text{ex}}) = \frac{n^2 E_{\text{ex}}^2}{\pi^2 \hbar^3 c^2} Q^2 S, \quad (13)$$

where

$$S = \frac{2e^2 \hbar |P_{cv}|^2}{\epsilon_0 c n m_0^2 E_{\text{ex}} a^3} \quad (14)$$

is the integrated intensity of the optical-absorption exciton-resonance spectra in bulk materials, and

$$Q = \int_0^\infty \frac{4t^2 f_c(t/a) [1 - f_v(t/a)]}{\pi(1+t^2)^2} dt. \quad (15)$$

Here, we used the relative-motion envelope wave function of $\phi(r) = 1/(\pi a^3)^{1/2} \exp(-r/a)$ (Ref. 41). We take P_{cv} at band edges. [In quantum wells, S is replaced by Eq. (22) in Sec. V. Q is modified to account for the two-dimensional motion of excitons.] In the steady state, the radiative recombination rate relates to the generation rate by

$$G = R(N_{\text{ex}}) + N_{\text{ex}}/\tau_{\text{NR}}, \quad (16)$$

where τ_{NR} is the nonradiative recombination lifetime. We assume that all photoexcited electron and hole pairs recombine through exciton states. Thus, the recombination lifetime of excitons is written as

$$\tau = N_{\text{ex}}/G, \quad (17)$$

and can be calculated as a function of G for a given τ_{NR} .

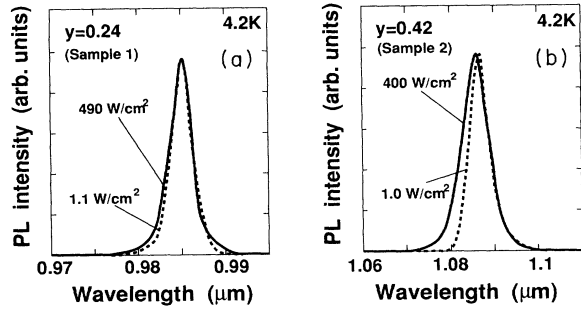


FIG. 6. (a) 4.2-K photoluminescence spectra of sample 1 at the excitation power of 490 W/cm² (solid line) and 1.1 W/cm² (dashed line). (b) 4.2-K photoluminescence spectra of sample 2 at the excitation power of 400 W/cm² (solid line) and 1.0 W/cm² (dashed line).

Figure 7 shows the calculated exciton lifetime at 4.2 K for $y=0.5$ In_{1-x}Ga_xAs_yP_{1-y} as a function of the generation rate of excitons in the case of $\tau_{\text{NR}} = \infty$ and 1 ns. We evaluated $S = 24$ eV/cm in Eq. (14) using $a = 13.7$ nm and calculating P_{cv} by Kane's band model (see Ref. 27 for a detailed calculation). We used $0.057m_0$ as the electron's effective mass and $0.5m_0$ as the hole's effective mass for calculating the distribution function. As the generation rate exceeded 1×10^{25} cm⁻³s⁻¹, the exciton lifetime became saturated below 1 ns, which is due to the saturation of the exciton density over 1×10^{16} cm⁻³. The lifetime monotonically increased as the generation rate decreased. When the nonradiative recombination process became dominant, the lifetime became τ_{NR} as shown in the case of $\tau_{\text{NR}} = 1$ ns.

We can relate the excitation power density to the generation rate of excitons by

$$G = \frac{\eta(1-R)P}{\hbar\omega d}, \quad (18)$$

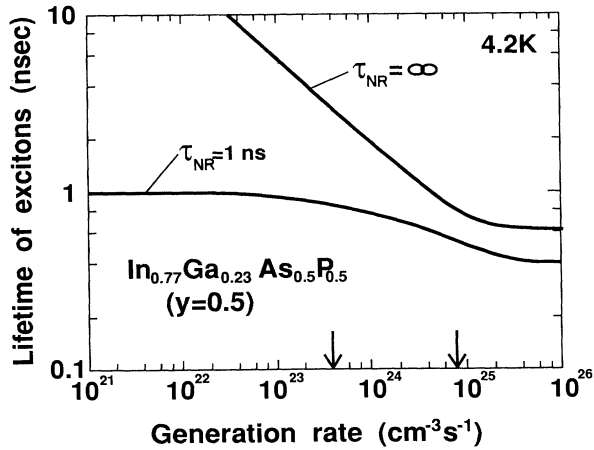


FIG. 7. Calculated lifetime of excitons at 4.2 K in bulk In_{0.77}Ga_{0.23}As_{0.5}P_{0.5} ($y=0.5$) as a function of the generation rate using the nonradiative recombination lifetime τ_{NR} of ∞ and 1 ns. The arrow at $G = 8 \times 10^{24}$ s⁻¹ cm⁻³ corresponds to the excitation power of $P = 200$ W cm⁻² and $G = 4 \times 10^{23}$ s⁻¹ cm⁻³ to $P = 10$ W cm⁻².

where R is the reflectivity, $\hbar\omega$ is the incident photon energy, d is the thickness of the In_{1-x}Ga_xAs_yP_{1-y} layer, and η is the quantum efficiency of the electron-hole pair generation in the In_{1-x}Ga_xAs_yP_{1-y} layers. We set the variables to $\hbar\omega = 1.92$ eV, $R = 0.3$, $\eta = 1$, and $d = 0.5$ μm . A power density of 200 W cm⁻², the higher critical point for spectrum width saturation, corresponds to the arrow at $G = 8 \times 10^{24}$ cm⁻³s⁻¹ in Fig. 7. The lower critical point, $P = 10$ W cm⁻², corresponds to the arrow at $G = 4 \times 10^{23}$ cm⁻³s⁻¹.

The close correlation between the measured spectrum width in Fig. 5 and the exciton lifetime at $\tau_{\text{NR}} = 1$ ns in Fig. 7, as a function of the excitation intensity, illuminates the features of exciton migration through macroscopically fluctuating alloys. When $P > 200$ W cm⁻², the exciton density becomes saturated in \mathbf{k} space, inhibiting the movement of excitons in real space. In this region, the spectrum broadening represents the spatial inhomogeneity of the exciton energy over the excited area. As the excitation power decreases, the number of excitons decreases from its saturation density, and excitons begin to migrate and recombine preferentially in the lower-energy region. This process makes the resonance spectrum asymmetric as observed in Fig. 6(b). When the exciton lifetime equals the nonradiative lifetime, the diffusion length becomes saturated and the spectrum stops narrowing. Sample 1 is expected to have almost homogeneous composition distributions and shows no spectrum change.

We can estimate the spatial size of macroscopic composition fluctuations from the diffusion length of excitons given by

$$L = \sqrt{D_{\text{ex}}\tau}. \quad (19)$$

The diffusion coefficient of excitons D_{ex} is given by Einstein's relation $D_{\text{ex}} = (kT/e)\mu_{\text{ex}}$, where k is Boltzmann's constant and μ_{ex} is the mobility of excitons. Setting $\mu_{\text{ex}} = 1000$ cm²V⁻¹s⁻¹, $T = 4.2$ K, and $\tau = 1$ ns, we obtain $L = 1900$ Å. This number represents the size of bulk materials with homogeneous composition. The saturated spectrum width at low excitation power density in samples 2 and 3 is still larger than the calculated statistical broadening. This shows that homogeneous composition regions exist with a somewhat larger extent.

To extend the composition fluctuation formula from bulk to quantum wells, we must take into account both the shrinkage of the exciton volume due to quantum confinement and the spread of the exciton wave function to the binary InP barriers in very thin quantum wells. Treating the variation in the band gap as the first-order perturbation of exciton energy, we derived the spectrum broadening in quantum wells as²⁷

$$\Gamma_{\text{QW}} = \left[\Gamma_{\text{sta}}^2 \left[\frac{V_{3\text{D}}}{V_{2\text{D}}} \right] + \Gamma_{\text{mac}}^2 \right]^{1/2} \times \left[\left[\frac{\partial E_c}{\partial E_g} \right] \langle \psi_e | \psi_e \rangle_{\text{well}} + \left[\frac{\partial E_v}{\partial E_g} \right] \langle \psi_h | \psi_h \rangle_{\text{well}} \right], \quad (20)$$

where V_{2D} is the two-dimensional exciton volume, $\partial E_c/\partial E_g$ represents the distribution of the band-gap change to the conduction band, and $\partial E_v/\partial E_g$ the distribution to the valence band. The integral is performed in $\text{In}_{1-x}\text{Ga}_x\text{As}_y\text{P}_{1-y}$ well regions. The contribution of the statistical composition fluctuation increases with the decrease of the well width due to the exciton shrinkage. We assume that broadening due to macroscopic composition fluctuation remains constant despite well width. We can calculate the exciton spectrum broadening in quantum wells using the magnitudes of statistical and macroscopic composition fluctuations in bulk layers. Singh and Bajaj⁴⁴ also derived a formula for the exciton spectrum broadening due to composition fluctuations in quantum wells. The major difference between our Eq. (20) and Eq. (8) in Ref. 44 is that we take into account the effects of exciton shrinkage and macroscopic composition fluctuation on spectrum broadening.

In Fig. 8, we illustrate the well-width dependence of the measured spectrum width (FWHM) taken from Fig. 3 on the calculated results for (a) $y=1.0$, (b) $y=0.9$, and (c) $y=0.6$ quantum wells. We use $V_{2D}=\pi L_w \lambda_{ex}^2$, where L_w is the well width and the two-dimensional exciton radius is variationally calculated as a function of the well width by Eq. (7). We took $\partial E_c/\partial E_g=0.4$. We used the reduced effective mass and the dielectric constant of bulk $\text{In}_{1-x}\text{Ga}_x\text{As}_y\text{P}_{1-y}$. The calculated width increases as the well width decreases to about 2 nm due to the shrinkage of exciton volume, and then decreases due to the spread of exciton wave function into InP barriers. In quantum wells with widths greater than about 5 nm, the measured spectrum width agrees well with the calculation, showing that spectrum broadening is dominated by composition fluctuations. In thinner quantum wells, the measured spectrum becomes broader than the calculation, which can be attributed to roughness at the interfaces. The substitution between the group-V atoms P and As during the growth interruption at interfaces is assumed to be the main cause for this spectrum broadening. This process is discussed in our previous works.^{17,27}

The open symbols in Fig. 8 represent the 4.2-K spectrum width (FWHM) in 20-period MQW's of each composition. The width of the wells are $L_w=10.3$ nm for $y=1.0$ MQW, $L_w=9.5$ nm for $y=0.9$ MQW, and $L_w=10.2$ nm for $y=0.6$ MQW. The spectrum width is only slightly larger than that of single quantum wells, showing that the broadening is dominated also by composition fluctuations. Figure 9 shows the excitation power dependence of the photoluminescence spectrum width in three MQW's at 4.2 K. As the excitation power decreases, the spectrum widths begin to decrease and saturate at critical power densities, showing the presence of macroscopic composition fluctuations in quantum wells as in bulk materials.

V. EXCITON OPTICAL-ABSORPTION SPECTRA

We presented a theoretical formula of the exciton-resonance optical-absorption spectrum in a previous work.²⁷ The optical absorbance of the spectrum in a quantum well is given by

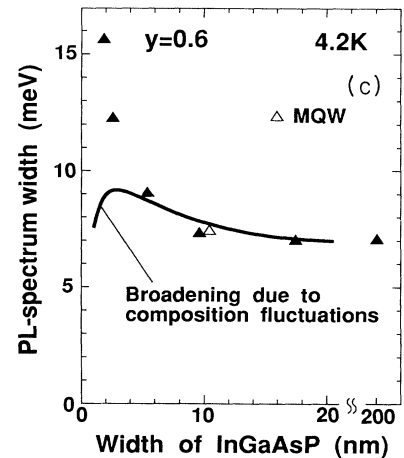
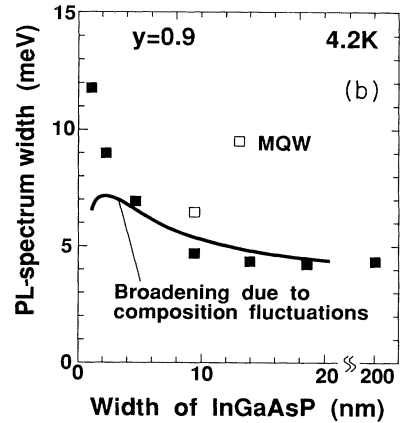
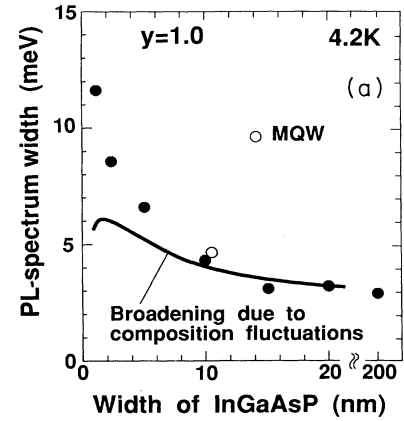


FIG. 8. Photoluminescence spectrum width (FWHM) at 4.2 K as a function of the width of $\text{In}_{1-x}\text{Ga}_x\text{As}_y\text{P}_{1-y}$ for (a) $y=1.0$, (b) $y=0.9$, and (c) $y=0.6$. The solid symbols represent the results of single quantum wells with InP barriers and bulk layers. The open symbols are the width in 20-period MQW's. Solid lines are the calculated spectrum width due to composition fluctuations by Eq. (20).

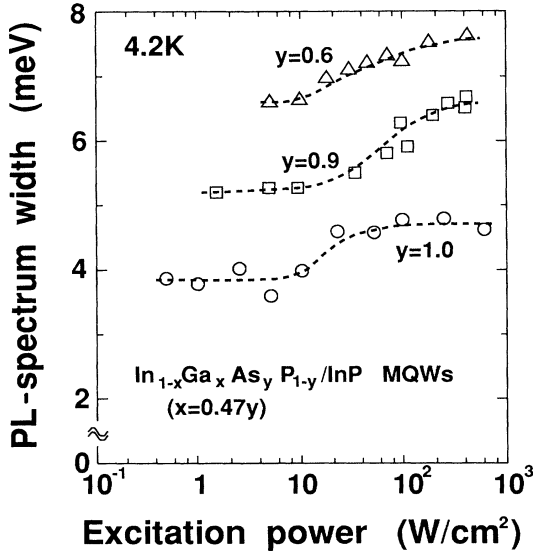


FIG. 9. Photoluminescence spectrum width (FWHM) of the three MQW's at 4.2 K as a function of the excitation power density.

$$\alpha_{\text{ex}}L_{\text{QW}} = SB(\hbar\omega - E_{\text{ex}}), \quad (21)$$

where

$$S = \frac{4e^2\hbar|P_{cv}|^2}{\epsilon_0 c n m_0^2 E_{\text{ex}} \lambda_{\text{ex}}^2} |\langle \psi_e(z) | \psi_h(z) \rangle|^2 \quad (22)$$

and

$$B(\hbar\omega - E_{\text{ex}}) = \int_{-\infty}^{\infty} B_0(\hbar\omega - E_{\text{ex}} + E) B_T(E) dE. \quad (23)$$

S is the integrated intensity of the resonance and $B(\hbar\omega - E_{\text{ex}})$ is the broadening function around the exciton energy. In Eq. (23), B_0 is the broadening function due to the inhomogeneity of the exciton energy and B_T is that due to the energy uncertainty of the exciton states that are quasistable by optical phonon scattering at high temperatures. We can represent a Gaussian distribution as B_0 . B_T can be described as

$$B_T(E) = \int_0^{\infty} \frac{f(\tau_s)}{\pi b} \frac{\sin^2(E/b)}{(E/b)^2} d\tau_s \quad (24)$$

with $b = 2\hbar/\tau_s$, where $f(\tau_s)$ represents the normalized distribution function of the exciton lifetime τ_s . In our previous work,²⁷ we found that $f(\tau_s)$ obeys a Lorentzian distribution with a FWHM of half the average in $\text{In}_{0.53}\text{Ga}_{0.47}\text{As}/\text{InP}$ quantum wells.

Figure 10 shows (a) 77-K and (b) 295-K optical-absorption spectra of $\text{In}_{1-x}\text{Ga}_x\text{As}_y\text{P}_{1-y}/\text{InP}$ MQW's with compositions of $y=0.6, 0.9,$ and 1.0 , whose low-temperature photoluminescence spectra were studied in Figs. 8 and 9. Due to the decrease in the band gap of the well layers, the absorption edge shifted toward a longer wavelength as the temperature and the arsenic composition increased. We can observe resonance spectra of the ground-state electron-heavy-hole excitons at the absorption edges and of the electron-light-hole excitons over

the steplike absorption continuum. Taking the peak of the spectra as the exciton energy and using the low-energy side of the spectra, we extracted the contribution of the electron-heavy-hole exciton resonance.

The integrated intensity of the resonance spectrum, represented by the shaded regions in Fig. 10(a), depends little on temperature and is a parameter specific in each quantum well as we have shown previously.²⁷ The measured values at 77 K are 1.06×10^{-4} eV in the $y=1.0$ MQW, 1.01×10^{-4} eV in the $y=0.9$ MQW, and 1.26×10^{-4} eV in the $y=0.6$ MQW.

We calculated the integrated intensity using Eq. (22) for the three quantum wells:

$$S = 2.32 \times 10^{-2} / \lambda_{\text{ex}}^2 \text{ eV} \quad (y=1.0), \quad (25)$$

$$S = 2.15 \times 10^{-2} / \lambda_{\text{ex}}^2 \text{ eV} \quad (y=0.9), \quad (26)$$

$$S = 1.75 \times 10^{-2} / \lambda_{\text{ex}}^2 \text{ eV} \quad (y=0.6), \quad (27)$$

where λ_{ex} is in nanometers. The detail in the calculation is described in Ref. 27. Substituting the measured integrated intensity into the above formula, we obtain the two-dimensional exciton radius for the three quantum wells: $\lambda_{\text{ex}} = 14.8$ nm for $y=1.0$ MQW, $\lambda_{\text{ex}} = 14.5$ nm for $y=0.9$ MQW, $\lambda_{\text{ex}} = 11.8$ nm for $y=0.6$ MQW.

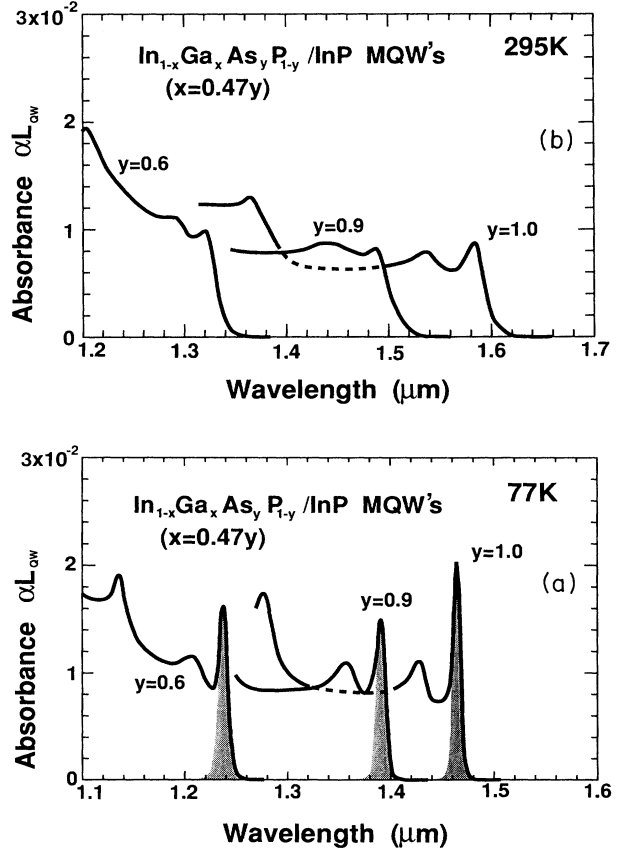


FIG. 10. Optical-absorption spectra of 20-period $\text{In}_{1-x}\text{Ga}_x\text{As}_y\text{P}_{1-y}/\text{InP}$ MQW's at (a) 77 K and (b) 295 K. The well and barrier layers are about 10 nm thick. The composition is $y=1.0, 0.9,$ and 0.6 with $x=0.47y$.

Figure 11 shows the measured integrated intensities and the calculated two-dimensional exciton radii as a function of the room-temperature band gaps of well materials. In addition to the three $\text{In}_{1-x}\text{Ga}_x\text{As}_y\text{P}_{1-y}/\text{InP}$ MQW's, we also plotted the integrated intensity of 1.6×10^{-4} eV in 10-nm $\text{GaAs}/\text{Al}_{0.25}\text{Ga}_{0.75}\text{As}$ quantum wells reported by Masselink *et al.*³⁹ and the radius of 9.7 nm, which we calculated.²⁷ As the band gap increases, the integrated intensity increases from 1.06×10^{-4} eV in $\text{In}_{0.53}\text{Ga}_{0.47}\text{As}$ to about 1.5 times this in GaAs. The two-dimensional exciton radius decreases from 14.8 nm in $\text{In}_{0.47}\text{Ga}_{0.53}\text{As}$ to 9.7 nm in GaAs. The smaller integrated intensity in long-wavelength $\text{In}_{1-x}\text{Ga}_x\text{As}_y\text{P}_{1-y}/\text{InP}$ quantum wells is primarily due to the larger exciton radius, rather than to GaAs quantum wells. The exciton radius is related to both the static dielectric constant and the in-plane reduced effective mass as can be seen in Eq. (7). Thus, the band-gap dependence of these two material parameters explains that of the radius.

The exciton spectrum profile at 77 K obeyed a Gaussian distribution with a FWHM of 4.7 meV for $y=1.0$, 6.3 meV for $y=0.9$, and 7.2 meV for $y=0.6$ MQW. These values agree with the photoluminescence spectrum width at 4.2 K measured at high excitation power as seen in Fig. 9. This shows that the inhomogeneous broadening dominates spectrum broadening and that the effect of thermal broadening can be neglected at this low temperature. At room temperature, the exciton spectrum broadened further to 11 meV in $y=1.0$ MQW, 12.5 meV in $y=0.9$ MQW, and 14 meV in $y=0.6$ MQW. In the $\text{In}_{0.53}\text{Ga}_{0.47}\text{As}/\text{InP}$ quantum wells,²⁷ the spectrum profile could be explained by Eqs. (23) and (24) assuming that the average exciton lifetime was 300 fs. We could not find any significant differences in the thermal broadening function between the three MQW's. Thus, the difference in the spectrum broadening up to room temperature is primarily caused by the differences in the magnitudes of composition fluctuations.

The optical absorbance of the exciton resonance is proportional to the integrated intensity and is approximately the inverse of the width of the broadening function. Thus, we can say that the exciton's optical-absorption strength in $\text{In}_{1-x}\text{Ga}_x\text{As}_y\text{P}_{1-y}/\text{InP}$ quantum wells varies as a function of the composition depending on the two-dimensional exciton radius and the magnitude of composition fluctuations.

VI. CONCLUSION

We systematically studied the optical characteristics of the ground-state electron-heavy-hole excitons in $\text{In}_{1-x}\text{Ga}_x\text{As}_y\text{P}_{1-y}/\text{InP}$ quantum wells grown by MOVPE. We specifically focused on the resonance energy, spatial energy inhomogeneity, and optical-absorption strength.

The optical absorbance of the exciton resonance spec-

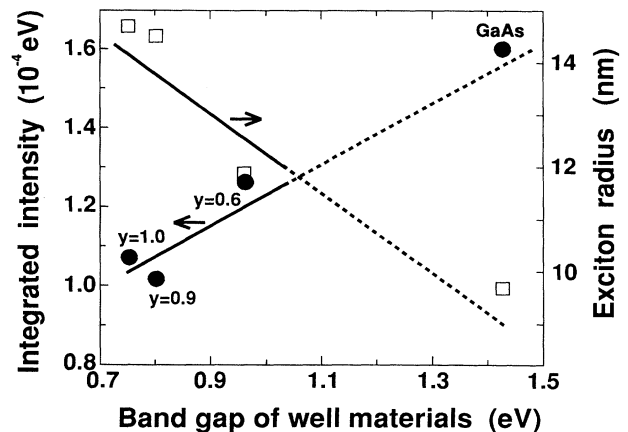


FIG. 11. The solid circles represent the measured integrated intensity of the ground-state electron-heavy-hole exciton resonance as a function of the room-temperature band gap of well materials. The values for the $\text{GaAs}/\text{Al}_{0.3}\text{Ga}_{0.7}\text{As}$ quantum wells are from Ref. 39. The open squares are the calculated two-dimensional exciton radius using the measured integrated intensity from Eqs. (22) and (25)–(27).

trum in quantum wells is described by the product of the integrated intensity and the normalized broadening function around the resonance energy. The exciton resonance energy can be tuned between the $\text{In}_{0.53}\text{Ga}_{0.47}\text{As}$ and InP band gap by controlling the composition and/or the width of the $\text{In}_{1-x}\text{Ga}_x\text{As}_y\text{P}_{1-y}$ wells. Its wavelength is what is needed for optical communication system devices. The inhomogeneous broadening of the resonance spectrum is primarily caused by two kinds of composition fluctuations in $\text{In}_{1-x}\text{Ga}_x\text{As}_y\text{P}_{1-y}$ wells: the statistical composition fluctuations that occur over the extent of exciton envelope wave functions, giving the lowest limit on the inhomogeneous broadening; the macroscopic composition fluctuations with about 1% in the group-III and/or group-V species. Based on the analysis of the excitation power dependence of the low-temperature photoluminescence spectrum, the size of the homogeneous composition area was estimated to be about a few thousand angstroms in our $\text{In}_{1-x}\text{Ga}_x\text{As}_y\text{P}_{1-y}$. We also found the integrated intensity of the resonance spectrum increased as the band gap of the well materials increased. This band-gap dependence correlates with that of the two-dimensional exciton radius. The optical absorbance of the exciton resonance in $\text{In}_{1-x}\text{Ga}_x\text{As}_y\text{P}_{1-y}/\text{InP}$ varies with the composition depending on both the two-dimensional exciton radius and the magnitude of the composition fluctuations.

ACKNOWLEDGMENTS

We wish to thank Dr. T. Sakurai and Dr. H. Imai for the many helpful discussions related to this paper.

- ¹L. Esaki and R. Tsu, *IBM J. Res. Dev.* **14**, 61 (1970).
- ²D. S. Chemla, D.A.B. Miller, and P. W. Smith, *Semiconductor and Semimetals* (Academic, New York, 1987), Vol. 24, Chap. 5.
- ³T. Ishibashi, S. Tarucha, and H. Okamoto, *Proceedings of the International Symposium on GaAs and Related Compounds, Oiso, 1981*, IOP Conf. Proc. No. 63 (Institute of Physics and Physical Society, London, 1981), p. 587.
- ⁴D.A.B. Miller, D. S. Chemla, T. C. Damen, A. C. Gossard, W. Wiegmann, T. H. Wood, and C. A. Burrus, *Phys. Rev. Lett.* **53**, 2173 (1984).
- ⁵D. A. B. Miller, D. S. Chemla, D. J. Eilenberger, P. W. Smith, A. C. Gossard, and W. T. Tsang, *Appl. Phys. Lett.* **41**, 679 (1982).
- ⁶T. H. Wood, C. A. Burrus, D. A. B. Miller, D. S. Chemla, T. C. Damen, A. C. Gossard, and W. Wiegmann, *Appl. Phys. Lett.* **44**, 16 (1984).
- ⁷D. A. B. Miller, D. S. Chemla, T. C. Damen, A. C. Gossard, W. Wiegmann, T. H. Wood, and C. A. Burrus, *Appl. Phys. Lett.* **45**, 13 (1984).
- ⁸D. A. B. Miller, D. S. Chemla, T. C. Damen, T. H. Wood, C. A. Burrus, A. C. Gossard, and W. Wiegmann, *IEEE J. Quantum Electron.* **QE-21**, 1462 (1985).
- ⁹H. M. Gibbs, S. S. Tarng, J. L. Jewell, D. A. Weinberger, K. Tai, A. C. Gossard, S. L. McCall, A. Passner, and W. Wiegmann, *Appl. Phys. Lett.* **41**, 221 (1982).
- ¹⁰H. Temkin, D. Gershoni, and M. B. Panish, *Appl. Phys. Lett.* **50**, 1776 (1987).
- ¹¹M. Razeghi, J. P. Hirtz, U. O. Ziemelis, C. Delalande, B. Etienne, and M. Voos, *Appl. Phys. Lett.* **43**, 585 (1983).
- ¹²J. H. Marsh, J. S. Roberts, and P. A. Claxton, *Appl. Phys. Lett.* **46**, 1161 (1985).
- ¹³C. P. Kuo, K. L. Fry, and G. B. Stringfellow, *Appl. Phys. Lett.* **47**, 855 (1985).
- ¹⁴M. S. Skolnick, P. R. Tapster, S. J. Bass, N. Apsley, A. D. Pitt, N. G. Cullis, S. P. Aldred, and C. A. Warwick, *Appl. Phys. Lett.* **48**, 1455 (1986).
- ¹⁵B. I. Miller, E. F. Schubert, U. Koren, A. Ourmazd, A. H. Dayem, and R. J. Capik, *Appl. Phys. Lett.* **49**, 1384 (1986).
- ¹⁶H. Kamei, T. Katsuyama, K. Ono, and K. Yoshida, *Proceedings of the 15th International Symposium on GaAs and Related Compounds*, IOP Conf. Proc. No. 96 (Institute of Physics and Physical Society, London, 1988), p. 125.
- ¹⁷M. Sugawara, T. Fujii, S. Yamazaki, and K. Nakajima, *Appl. Phys. Lett.* **54**, 1353 (1989).
- ¹⁸P. J. A. F. Thijs, E. A. Montie, H. W. van Kesteren, and G. W. 't Hooft, *Appl. Phys. Lett.* **53**, 971 (1988).
- ¹⁹M. Kondo, S. Yamazaki, M. Sugawara, H. Okuda, K. Kato, and K. Nakajima, *J. Cryst. Growth* **93**, 376 (1988).
- ²⁰M. B. Panish, H. Temkin, R. A. Hamm, and S. N. G. Chu, *Appl. Phys. Lett.* **49**, 164 (1986).
- ²¹H. Temkin, M. B. Panish, P. M. Petroff, R. A. Hamm, J. M. Vandenberg, and S. Sumski, *Appl. Phys. Lett.* **47**, 394 (1985).
- ²²W. T. Tsang and E. F. Schubert, *Appl. Phys. Lett.* **49**, 220 (1986).
- ²³M. S. Skolnick, L. L. Taylor, S. J. Bass, A. D. Pitt, D. J. Mowbray, A. G. Cullis, and N. G. Chew, *Appl. Phys. Lett.* **51**, 24 (1987).
- ²⁴H. Temkin, D. Gershoni, and M. B. Panish, *Appl. Phys. Lett.* **50**, 1776 (1987).
- ²⁵K. Wakita, Y. Kawamura, Y. Yoshikuni, H. Asahi, and S. Uehara, *IEEE J. Quantum Electron.* **QE-22**, 1831 (1986).
- ²⁶I. Bar-Joseph, C. Klingshirn, D. A. B. Miller, D. S. Chemla, U. Koren, and B. I. Miller, *Appl. Phys. Lett.* **50**, 1010 (1987).
- ²⁷M. Sugawara, T. Fujii, S. Yamazaki, and K. Nakajima, *Phys. Rev. B* **42**, 9587 (1990).
- ²⁸M. Sugawara, M. Kondo, S. Yamazaki, and K. Nakajima, *J. Cryst. Growth* **93**, 318 (1988).
- ²⁹M. Sugawara, M. Kondo, S. Yamazaki, and K. Nakajima, *Appl. Phys. Lett.* **52**, 742 (1988).
- ³⁰B. Deveaud, J. Shah, T. C. Damen, and W. T. Tsang, *Appl. Phys. Lett.* **52**, 1886 (1988).
- ³¹M. Gal, C. P. Kuo, B. Lee, R. Ranganathan, P. C. Taylor, and G. B. Stringfellow, *Phys. Rev. B* **34**, 1356 (1986).
- ³²D. S. Chemla, D. A. B. Miller, P. W. Smith, A. C. Gossard, and W. Wiegmann, *IEEE J. Quantum Electron.* **QE-20**, 265 (1984).
- ³³M. Zachau and D. Grutzmacher, *Appl. Phys. Lett.* **56**, 632 (1990).
- ³⁴P. C. Morais, H. M. Cox, P. L. Bastos, D. M. Hwang, J. M. Worlock, E. Yablonoitch, and R. E. Nahory, *Appl. Phys. Lett.* **54**, 442 (1989).
- ³⁵D. A. B. Miller, D. S. Chemla, T. C. Damen, A. C. Gossard, W. Wiegmann, T. H. Wood, and C. A. Burrus, *Phys. Rev. B* **32**, 1043 (1985).
- ³⁶S. R. Forrest, P. H. Schmidt, R. B. Wilson, and M. L. Kaplan, *Appl. Phys. Lett.* **45**, 1199 (1984).
- ³⁷T. P. Pearsall, *GaInAsP Alloy Semiconductors* (Wiley, New York, 1982) p. 456.
- ³⁸S. Adachi, *J. Appl. Phys.* **53**, 8775 (1982).
- ³⁹W. T. Masselink, P. J. Pearsall, J. Klem, C. K. Peng, H. Morokoc, G. D. Sanders, and Yia-Chung Chang, *Phys. Rev. B* **32**, 8027 (1985).
- ⁴⁰E. F. Schubert, E. O. Göbel, Y. Horikoshi, K. Ploog, and H. J. Queisser, *Phys. Rev. B* **30**, 813 (1984).
- ⁴¹J. O. Dimmock, *Semiconductor and Semimetals* (Academic, New York, 1967), Vol. III, Chap. 7.
- ⁴²E. F. Schubert and W. T. Tsang, *Phys. Rev. B* **34**, 2991 (1986).
- ⁴³H. C. Casey, Jr. and M. B. Panish, *Heterostructure Lasers* (Academic, New York, 1978), Chap. 3.
- ⁴⁴J. Singh and K. K. Bajaj, *J. Appl. Phys.* **57**, 5433 (1985).